Published online 20 April 2021

Nucleic Acids Research, 2021, Vol. 49, No. 13 ***e74***
https://doi.org/10.1093/nar/gkab262

Measuring nonhomologous end-joining, homologous recombination and alternative end-joining simultaneously at an endogenous locus in any transfectable human cell

Suleman S. Hussain[1], Rahul Majumdar[1], Grace M. Moore[1], Himanshi Narang[1], Erika S. Buechelmaier[1,2], Maximilian J. Bazil[1], Pavithran T. Ravindran[3], Jonathan E. Leeman[4], Yi Li[1], Manisha Jalan[1], Kyrie S. Anderson[1], Andrea Farina[5], Rekha Soni[5], Neeman Mohibullah[5], Edin Hamzic[6], Xiaoqing Rong-Mullins[7], Christopher Sifuentes[8], Rama R. Damerla[1], Agnes Viale[5], Simon N. Powell[1] and Daniel S. Higginson[1,*]

[1]Department of Radiation Oncology, Memorial Sloan Kettering Cancer Center, New York, NY 10065, USA, [2]Weill Cornell Medicine, Graduate School of Medical Sciences, New York, NY 10065, USA, [3]Princeton University, Princeton, NJ 08544, USA, [4]Department of Radiation Oncology, Dana-Farber Cancer Institute, Harvard Medical School, Boston, MA 02189, USA, [5]Integrated Genomics Operations, Memorial Sloan Kettering Cancer Center, New York, NY 10065, USA, [6]Biocomputix, Sarajevo, 71000, Bosnia and Herzegovina, [7]Department of Biostatistics, The Ohio State University College of Public Health, Columbus, OH 43210, USA and [8]Takara Bio USA, Inc., Mountain View, CA 94043, USA

Received November 10, 2020; Revised March 23, 2021; Editorial Decision March 29, 2021; Accepted April 01, 2021

ABSTRACT

Double strand break (DSB) repair primarily occurs through 3 pathways: non-homologous end-joining (NHEJ), alternative end-joining (Alt-EJ), and homologous recombination (HR). Typical methods to measure pathway usage include integrated cassette reporter assays or visualization of DNA damage induced nuclear foci. It is now well understood that repair of Cas9-induced breaks also involves NHEJ, Alt-EJ, and HR pathways, providing a new format to measure pathway usage. Here, we have developed a simple Cas9-based system with validated repair outcomes that accurately represent each pathway and then converted it to a droplet digital PCR (ddPCR) readout, thus obviating the need for Next Generation Sequencing and bioinformatic analysis with the goal to make Cas9-based system accessible to more laboratories. The assay system has reproduced several important insights. First, absence of the key Alt-EJ factor Pol θ only abrogates ∼50% of total Alt-EJ. Second, single-strand templated repair (SSTR) requires BRCA1 and MRE11 activity, but not BRCA2, establishing that SSTR commonly used in genome editing is not conventional HR. Third, BRCA1 promotes Alt-EJ usage at two-ended DSBs in contrast to BRCA2. This assay can be used in any system, which permits Cas9 delivery and, importantly, allows rapid genotype-to-phenotype correlation in isogenic cell line pairs.

INTRODUCTION

Double strand breaks (DSBs) can be generated spontaneously through oxidative stress accumulated during cellular respiration or exogenously from cosmic rays and therapeutic radiation used to treat 50% of all cancer patients (1). These breaks result in two double-stranded DNA ends on either side of the breaksite and are repaired primarily through two pathways: nonhomologous end-joining (NHEJ) and homologous recombination (HR). However,

*To whom correspondence should be addressed. Tel: +1 646 888 3567; Email: higginsd@mskcc.org
Present addresses:
Himanshi Narang, Bhabha Atomic Research Centre, Mumbai, India.
Yi Li, Department of Oncology, Kunming General Hospital, Kunming, China.
Kyrie S. Anderson, Weill Cornell Medicine, New York, NY, USA.
Rama R. Damerla, Kasturba Medical College Manipal, Manipal Academy of Higher Education, Manipal, India.

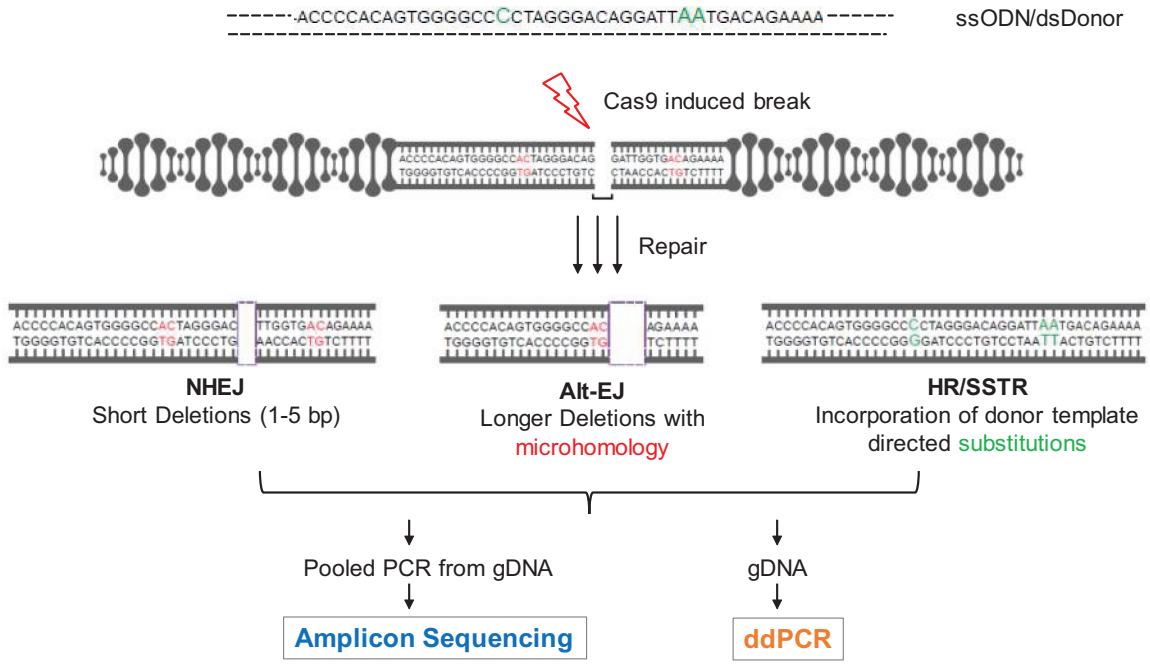

Figure 1. Schema of approach. Cas9 and gRNA expression plasmids are transfected into a cell population with or without a DNA donor sequence. Both single stranded oligonucleotide donors (ssODN) and double stranded DNA donors (dsDonor) with 3 substitutions (in green) are used in this study. NHEJ is classified as short deletions ranging from 1–5 bp and Alt-EJ is categorized by at least 5 bp deletion with at least 2 bp MH (representative 2 bp MH shown in red). Following an incubation period of typically 2–3 days, a range of repair pathway usage are assessed using PCR amplification of a 201 bp segment around the break followed by sequencing of the PCR product with paired end 150 × 2 Illumina MiSeq sequencing (Amplicon Sequencing). Alternatively, genomic DNA is used as an input for droplet digital PCR (ddPCR) to measure specific repair products on a Biorad QX200 platform.

there are additional backup pathways, such as alternative end-joining (Alt-EJ) which is mediated through polymerase theta (Pol θ, gene name *POLQ*) (2,3). Alt-EJ is particularly important in certain contexts, such as in tumor cells deficient in homologous recombination due to *BRCA1/2* mutations (2,3) or in cancers associated with the human papillomavirus (4–6).

Specialized reporter assays, wherein a non-functional fluorescent protein expression cassette is incorporated into a cell genome, are among the most commonly used tools to measure each DNA repair pathway in human cell lines. A break is created within the expression cassette, stimulating repair and restoring the expression of the fluorescent protein if a given repair pathway is employed. For instance, the DR-GFP system restores GFP expression if HR is used to repair a break (7); the EJ2-GFP system similarly measures Alt-EJ (8); the EJ5-GFP system uses two distal breaks to differentiate canonical NHEJ and Alt-EJ based on the restoration of an I-SceI cut site (8); and the EJ7-GFP system which can be modified to measure both NHEJ and Alt-EJ (9). Also, the EJ-RFP system can measure NHEJ separately and the EJ-DR system measures HR as well as any mutagenic end-joining event at an I-SceI site (10,11). To our knowledge, no single system measures all three pathways (NHEJ, HR, and Alt-EJ) in human cells. Moreover, in each case, the assays are limited to specialized cell line clones with stably integrated reporter cassettes.

Cas9 breaks at an endogenous locus have been used to capture repair by Pol θ (Alt-EJ) and KU70 (NHEJ) in mouse cells as previously described (12,13). Similarly, profiles of insertions and deletions along with their corresponding MH have been characterized at multiple Cas9 break sites using Next Generation Sequencing in various human cell lines (14–17). However, the ability to clearly differentiate Alt-EJ from NHEJ poses a significant challenge. Resection is generally considered the distinguishing factor between NHEJ and Alt-EJ; but differences in the use of microhomology (MH) between these pathways are still unclear. Notably, NHEJ can also use up to 3 bp MH for repair (9) and Alt-EJ may utilize as few as 2 bp of MH (18,19). Recent evidence suggests that Pol θ promotes deletions with 2 bp MH while reducing those with only 0–1 bp MH (13). We sought to categorize deletions at an endogenous breaksite as either NHEJ-dependent or Alt-EJ-dependent by using controls and isogenic cell line pairs. Our goal was to design a system that could employ Cas9 breaks to differentiate DSB repair pathways and could be easily applied across multiple cell lines.

We present a method to simultaneously measure multiple DNA DSB repair pathways using a Cas9-generated break at the AAVS1 genomic locus. Intending to expand this system's comprehensiveness to include HR, we co-transfected cells with a homologous donor with three mutations. Genomic DNA is collected after cells undergo repair of the Cas9-generated break (Figure 1). This is followed by PCR amplification of a 201 bp product around the break site which is size selected and sequenced using paired-end Illumina based Next Generation Sequencing (NGS). The NGS data is processed through a bioinformatic pipeline developed to classify reads into NHEJ, Alt-EJ and HR pathways considering deletion size and MH usage around the break site. Upon validating the method using appropriate

pathway controls (isogenic pairs of wild type and pathway deficient gene knockouts and pharmacological inhibitors), we identified characteristic reads for each of the pathways (NHEJ, Alt-EJ and HR/SSTR). These single reads were then converted to a simpler droplet digital PCR (ddPCR) format that allows for the quantification of DSB repair pathways by measuring the absolute value of their respective characteristic read. Overall, this assay is capable of quantifying NHEJ, Alt-EJ and HR simultaneously and in multiple cell contexts.

Using this system, we corroborate a few biological insights. First, the use of single stranded oligonucleotide donors (ssODNs) in Cas9 systems, although frequently described to use homology directed repair, requires BRCA1 but not BRCA2. Second, we demonstrate wide variation in Alt-EJ usage at an endogenous locus across cell lines, but consistent partial, not complete, dependence on Pol θ. Third, we observe that Alt-EJ, generally considered as a back-up pathway in HR deficiency, is suppressed in the absence of BRCA1.

MATERIALS AND METHODS

Reagents

Reagents, commercial kits, and drugs	Source	Catalog number
Lipofectamine 3000 reagent	Thermo	Cat #: 21341
Q5 Hot Start High-fidelity 2X Mastermix	New England Biolabs	Cat #: M0494
Mirin	Cayman Chemicals	Cat #:13208
Palbociclib	Millipore Sigma	Cat #: PZ0199
NU7441	SelleckChem	Cat #: S2638
DNeasy Kit	Qiagen	Cat #: 69506
Monarch PCR Clean-up Kit	NewEngland Biolab	Cat #: T1030S
E-gel Electrophoresis kit	ThermoFisher	Cat #: G661012
EnGen® Mutation Detection Kit	NewEngland Biolab	Cat #: E3321S

Biological resources

Cell lines, plasmids and si-RNA	Source	Catalog number
HAP1 WT	Horizon Discovery	Cat #: C631
HAP1 *POLQ*^{KO}	Horizon Discovery	Cat #: HZGHC000647c005
HAP1 *LIG4*^{KO}	Horizon Discovery	Cat #: HZGHC000759c005
HAP1 *RAD52*^{KO}	Horizon Discovery	Cat #: HZGHC000623c002
DLD-1 WT	Horizon Discovery	Cat #: CCL-221
DLD-1 BRCA2 KO	Horizon Discovery	Cat #: HD 105–007
U2OS WT	Gift from Jeremy Stark (20)	NA
U2OS *POLQ*^{KO}	Gift from Jeremy Stark (20)	NA
U2OS *RAD52*^{KO}	Gift from Jeremy Stark (20)	NA
U2OS EJ-2	Gift from Jeremy Stark (8)	NA
HCC1937 pcDNA3.1	Previous publication (21)	NA
HCC1937 BRCA1 complemented	Previous publication (21)	NA
HEK293T	ATCC	Cat #: CRL-3216
AAVS1 T2 CRISPR in pX330	Addgene	Cat #: 72833
pUC57 DS-121	Made for this paper (Genscript)	N/A
ON-TARGETplus Human BRCA1 (672) siRNA - SMARTpool	Dharmacon	Cat #: L-003461
ON-TARGETplus Non-targeting siRNA #1	Dharmacon	Cat #: D-001810

Computational resources

Software and algorithms	Source	Link
Graphpad Prism 8	GraphPad	
Code for Sequencing	Github	https://github.com/cjsifuen/delmh

Quantification and statistical analysis

For all statistical analyses, a two-tailed *P*-value of <0.05 was considered statistically significant. Statistical analyses were performed using Prism 8 (GraphPad Software, Inc.).

Contact for reagent and resource sharing

Requests for reagents and resources should be made by contacting Daniel Higginson, MD (higginsd@mskcc.org). Plasmids can be obtained through addgene.org or by contacting the lead author, as per table.

Cell culture

HAP1 (WT, *POLQ*^{KO}, *LIG4*^{KO}, *RAD52*^{KO}) cells were cultured in IMDM medium and DLD-1 (WT, BRCA2^{KO}) cells were cultured in RPMI media. U2OS (WT, *POLQ*^{KO}, *RAD52*^{KO}, EJ2) and HEK239T were cultured in DMEM medium. HCC1937 (pcDNA3.1 and BRCA1 complemented) were grown in IMDM media with 150 μg/ml G418 as previously described (21). All media was supplemented with 10% FBS, 2.5 mM L-glutamine and 100 μg/ml Penicillin/Streptomycin.

CRISPR/Cas9 plasmid transfection

0.15–0.25×10∧6 cells/well were plated in a six-well plate and were transfected the following day with 2 μg of CRISPR plasmid (measured by Nanodrop) directed at the AAVS1 locus using Lipofectamine 3000. A 121 bp donor template oligonucleotide with three substitutions was purchased from IDT and transfected with the Cas9. 1 μl of 10 μM donor oligo was added to each Lipofectamine 3000 tube with the CRISPR plasmid to measure SSTR. DSTR was assessed by cloning the same 121 bp donor sequence in the pUC57 plasmid for which 2 μg was added in each Lipofectamine 3000 tube. AAVS1 T2 CRISPR in pX330 was a gift from Masato Kanemaki (Addgene plasmid # 72833) (22). Seventy-two hours following transfection, cells were harvested and gDNA was extracted using the Qiagen DNeasy kit.

ssODN sequence with the three substitutions highlighted:

CAGGGCCGGTTAATGTGGCTCTGGTTCTGGGT
ACTTTTATCTGTCCCCTCCACCCCACAGTGGG
GCC**C**CTAGGGACAGGATT**AA**TGACAGAAAAGC
CCCATCCTTAGGCCTCCTCCTTCCT

PCR amplification, DNA purification

250 ng of genomic DNA (measured using Nanodrop) was used in a 201 bp PCR reaction employing primers surrounding the expected breaksite (Forward Primer:CTCCAGGG ATCCTGTGTCC and Reverse Primer:ACAGGAGGTG

GGGGTTAGAC). Then the PCR product was purified through the Monarch PCR Clean-up Kit and purified further using the E-Gel electrophoresis system (ThermoFisher Scientific) to size-select for the 201 bp product. Cas9 cuts were confirmed using a T7 endonuclease assay for a 495 bp product around the breaksite (Supplementary Figure S1).

Next generation sequencing and bioinformatics

400 ng of the 201 bp PCR product was submitted to the MSKCC Integrated Genomics Operations core for paired end P150 Illumina MiSeq Sequencing. We received at least 60 000 reads per sample and stitching of the paired reads was performed using the PEAR software requiring a minimum overlap of 10 nucleotides as previously described (4) BLOSUM62 was used for alignment which is parameterized by a gap-open penalty of –10 and a gap extension penalty of –1. The alignment was used to identify deletions, insertions and substitutions in each stitched read with the lowest probability of occurring by chance. Microhomology was identified by searching for >2 bp sequence matches between the deleted site and the site flanking the break. DSB repair pathways were classified from the alignment as follows: (a) NHEJ for up to 5 bp deletion or 1 bp insertion, (b) Alt-EJ as >5 bp deletion and MH of >2 bp or (c) HR/SSTR if the read was detected with three 1-bp substitutions introduced with the donor.

Droplet digital PCR (ddPCR)

Primers and probes for ddPCR are listed below in Table 1. A constant REF probe was used in all assays away from the break site to count the number of droplets with DNA. FAM probes were designed using Primer3Plus and following the guidelines listed in the Bio-rad ddPCR handbook. Probes were designed to be specific to the WT sequence (WT probe), the 12 bp deletion sequence (Alt-EJ probe), the 1 bp deletion (NHEJ probe) or the 3 bp substitutions (HR probe). 20 ng of genomic DNA was used per well in triplicate for Alt-EJ, NHEJ and HR probes and 9 ng per well of DNA was used for the WT probe in duplicate. The gDNA was cut using BamHI to better separate droplets with the desired region of interest before ddPCR was performed. The reaction mixes were ordered through Bio-Rad (Hercules, CA, USA) and were performed on a QX200 ddPCR system (Bio-Rad) at the Integrated Genomics Core at MSKCC. Reactions were partitioned into a median of approximately 15 000 droplets per well using the QX200 droplet generator. Emulsified reactions were amplified on a 96-well thermal cycler using cycling conditions identified during the optimization step. Plates were read and analyzed using QuantaSoft software (Bio-Rad) to assess the number of positive droplets. The assay threshold sensitivity was set at two mutant droplets.

Deletion size and MH length analysis

BRCA1 and *BRCA2* mutational signatures analyses were conducted with data downloaded from the Pan-Cancer Analysis of Whole Genomes (PCAWG), a consortium of the International Cancer Genome Consortium (ICGC) and The Cancer Genome Atlas (TCGA) (https://dcc.icgc.org/releases/PCAWG). Instructions for accessing data are available at https://docs.icgc.org/pcawg/data/. Of PCAWG's 2780 whole cancer genomes, only white-listed breast, ovarian, prostate and pancreatic cancers with biallelic mutations were analyzed (585 samples). These genomes were paired with single base substitution (SBS) and indel (ID) signature calls generated by Alexandrov *et al*. using SigProfiler (23). Samples were identified as having biallelic *BRCA1* or *BRCA2* driver mutations using previous mutation calls (24). Wild-type (WT) samples were defined as any remaining breast, ovarian, prostate, or pancreatic sample with a biallelic mutation in genes other than *BRCA1* or *BRCA2*. Large-scale state transitions (LST), a marker of HRD, were determined for all WT, BRCA1 and BRCA2 samples using a modified version of the *calc.lst( )* function from the Signature Tools Lib R package (25,26). Templated insertions (TINS), a signature of Pol θ activity, were also identified for all samples using a Python script developed by the lab based on the methods of Carvajal-Garcia *et al*., scanning 50 bp on either side of an insertion looking for direct or inverse repeats (13). Proportions of SBS3, ID6 and ID8 signatures were calculated in *WT*, *BRCA1* and *BRCA2* groups. SBS3 is a signature identified by a flat distribution of base substitutions and is strongly associated with HRD (27) ID6 is predominately characterized by ≥5 bp deletions with ≥2 bp of microhomology, likely caused by Alt-EJ, while ID8 is predominately ≥5 bp deletions with <2 bp or no microhomology (23). Certain indel signatures were withheld from calculations because they are markers of events not relevant to DSB repair pathways. ID1 and ID2 were not included because they are caused by slippage events during DNA replication. ID7 is likely due to defective DNA mismatch repair and ID13 is likely the result of DNA damage induced by UV light, as such, they were alsoomitted. ID11 and ID16 were found to be predominately insertions and were not evaluated.

BRCA1 and *BRCA2* deletion size and microhomology length analyses were conducted with the same data downloaded from PCAWG (24). The same 585 cancer genomes were paired with deletion counts generated by Alexandrov *et. al.* and the same *BRCA1*, *BRCA2* and WT groups were used for this analysis (23). The classifications of deletions used by Alexandrov *et. al.* were changed to include the microhomology length in all deletion events. For example, an event classified as a 2 bp deletion in a sequence of two 2 bp repeats (e.g. GTTTC|**AC**|**AC**GCTG) was redefined as a 2 bp deletion with 2 bp of microhomology. Proportions of the new deletion classifications were then calculated in

Table 1. Primers and probes for ddPCR

Primer	Sequence
Forward primer	CTGGGACCACCTTATATTCCC
Reverse primer	TAGACCCAATATCAGGAGACTAGG
Assay	**Probe**
Reference (REF)	TTAATGTGGCTCTGGTTCTGGGT
WT	CTAGGGACAGGATTGGTGACAGAAAAG
NHEJ	CCACTAGGGACAGATTGGTGACA
Alt-EJ	CCACTAGGGACAGAAAAGCCC
HR	CCCTAGGGACAGGATTAATGACAGA

WT, *BRCA1* and *BRCA2* groups. A principal component analysis (PCA) was performed on these data and graphed in R. The PCA analysis of deletion size and MH length in m*BRCA1*, m*BRCA2* and WT tumors shows clustering of the m*BRCA1* and m*BRCA2* tumors around larger deletions (≥5 bp) with varying MH lengths and WT tumors cluster with 1-bp deletions with small MH (≤1 bp) (Supplementary Figure S2A). Taking a closer look at the relationship between m*BRCA1* and m*BRCA2*, there is a slight distinction between the tumor samples based on MH length; m*BRCA1* tumors lean toward larger deletions with smaller MH (≤1 bp) while m*BRCA2* tumors move towards larger deletions with larger MH (≥3 bp) (Supplementary Figure S2B). Statistical significance was determined with unpaired two-tailed Mann–Whitney test ($P \leq 0.05$) using Prism 8 (GraphPad Software).

RESULTS

Deletion profiling captures pathway trade-off between NHEJ and Alt-EJ and applies to a wide variety of cell types

To verify NHEJ and Alt-EJ pathway contributions to the various deletions after Cas9 cuts at the AAVS1 locus, we used several controls to differentiate each of these pathways. NHEJ controls included pharmacologic inhibition of DNA-PKcs, the kinase centrally involved in bridging the breaksite and recruiting other NHEJ factors, and a *LIG4*^{KO} control cell line as LIG4 is the key ligase active in the final step of NHEJ. Alt-EJ controls, we included *POLQ*^{KO}, a key factor involved in the removal of RPA, annealing of microhomologies, and polymerization functions involved in Alt-EJ. To impair resection, upstream of both Alt-EJ and HR, we utilized an MRE11 inhibitor (MRE11i) and also a CDK4/6 inhibitor to arrest cells in G1, wherein resection is downregulated.

Interestingly, HAP1 *LIG4*^{KO} cells and HEK293T cells treated with DNA-PKi show a sharp decline in smaller deletions and an increase in larger deletions compared to their respective control (Figure 2A and B). In contrast, HAP1 *POLQ*^{KO} and CDK4/6i treated cells showed an increased peak of smaller deletions and a decrease in larger deletions (Figure 2C and D). Upon collating all deletions of a particular size and plotting it against deletion frequency, clusters of deletion between 1–5 bp were significantly decreased in *LIG4*^{KO} cells and DNA-PKi treated cells (Figure 2E and F). Another cluster between 10 and 15 bp was diminished in *POLQ*^{KO} cells and after CDK4/6i treatment and enhanced after *LIG4*^{KO} and DNA-PKi treatment (Figure 2E–G).

Based on literature-derived criteria from previous work in mouse embryonic fibroblasts deficient in Ku and Pol θ, NHEJ is demarcated by 1–5 bp deletions with less than 2 bp MH usage while Alt-EJ deletions (mediated by Pol θ) are generally >5 bp with at least 2 bp MH surrounding the breaksite (12). These criteria were used to bin NHEJ and Alt-EJ deletions in our system. For example, DNA-PKi treatment in HEK293T cells decreased NHEJ repair events and in HAP1 *LIG4*^{KO} cells we saw an almost complete loss of NHEJ repair (Figure 2G). The comparatively smaller reduction in NHEJ after DNA-PKi corroborates previous reports of functional redundancy between DNA-PK and XLF to perform NHEJ repair (9,28). The Alt-EJ repair events were reduced to ∼50% in *POLQ*^{KO} cells, while NHEJ events remained mostly unchanged (Figure 2G and H). In absence of Pol θ, Alt-EJ repair events are likely traded off to HR instead of NHEJ, as both pathways are downstream of resection. Using an MRE11i to inhibit resection, we observed an almost complete loss of Alt-EJ repair events (Figure 2H). Similarly, arresting HAP1 WT cells in G1 using a CDK4/6i, which inhibits resection through upstream inactivation of CDK2-activation of CTIP (29), led to a sharp decline in Alt-EJ repair (Figure 2H). Similarly, Alt-EJ repair by the EJ-2 assay in U2OS-EJ2 cells is suppressed after G1 arrest (Supplementary Figure S3). Thus, Alt-EJ is resection and cell cycle dependent, while Pol θ inhibition does not lead to a complete abrogation of the Alt-EJ reads. Conversely, there was an increase in NHEJ repair events in HEK293T cells treated with CDK4/6i or MRE11i. As expected, there is severely reduced NHEJ repair in *LIG4*^{KO} cells relative to wild type cells and after DNA-PKi treatment in HEK293T cells (Figure 2G and H). We performed the assay in multiple cell lines derived from various sources (head and neck cancer, breast cancer, prostate, colon, etc.) and observed similar deletion patterns, supporting the wide applicability of this assay system (Figure 2I).

Single characteristic deletions are representative of Alt-EJ and NHEJ

To simplify analyses and broaden the availability of the technique to more laboratories, we identified single reads which were each characteristic of Alt-EJ and NHEJ. The most frequent deletion was a 1bp deletion which was significantly downregulated in HAP1 *LIG4*^{KO} cells and after treatment with DNA-PKi (Figure 3A). Additionally, this 1 bp deletion was increased after treatment with CDK4/6i and MRE11i (Figure 3B). The heatmap also depicts a range of 10–12 bp deletions associated with MH which were downregulated in *POLQ*^{KO} and after treatment with CDK4/6i and MRE11i (Figure 3B). The most prominent read was a 12 bp deletion with 5 bp MH. This 12 bp deletion was also increased in *LIG4*^{KO} cells and HEK293T cells treated with DNA-PKi (Figure 3A). As expected, there was an inverse relation of deletions mediated by LIG4 and Pol θ, with a cluster of smaller deletions representing NHEJ and the larger deletion cluster associated with MH usage representing Alt-EJ (Figure 3C). On performing principal component analysis (PCA) on these deletions using HAP1 WT, *POLQ*^{KO} and *LIG4*^{KO} controls, the 1 bp deletion and 12 bp deletion with 5 bp MH specifically separated as two different components (Figure 3D). Thus, we propose that the 1 bp deletion and 12 bp deletion with 5 bp of MH signatures identified by this assay are representative of these two repair pathways and could be used to differentiate them. To confirm that these single characteristic reads would be sufficient to study pathway tradeoffs we reproduced similar pathway shifts using these singular reads in the various isogenic controls and drug treatments for DSB repair pathways (Figure 3E and F, Supplementary Figure S4).

Previous reports have shown that *POLQ* knockdowns only partially decreases Alt-EJ in two different assay systems (2,3). Additionally, *POLQ*^{KO} clones in A549 cells showed about a 50% decrease in Alt-EJ signal using a Cas9

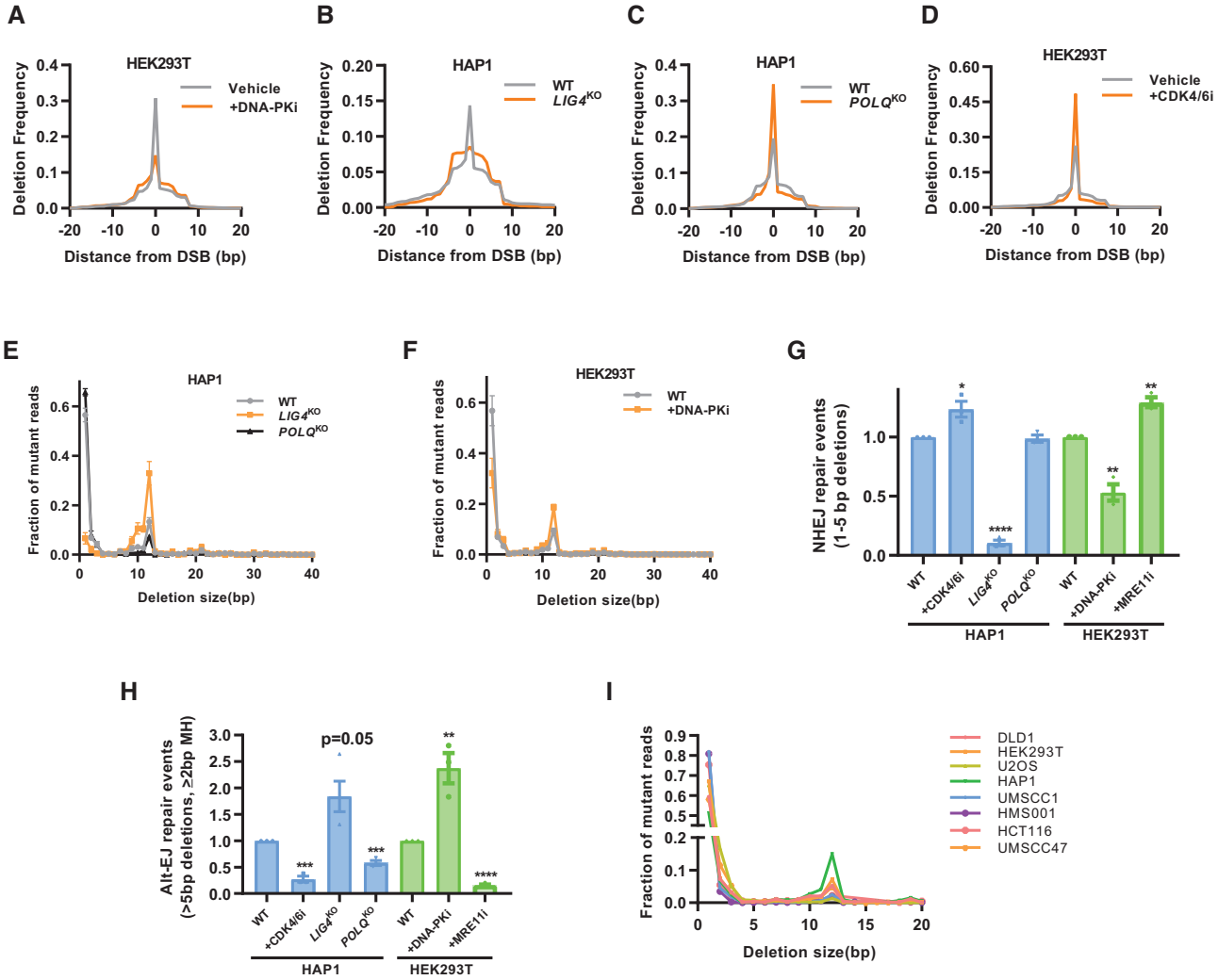

Figure 2. Cas9 induces patterned deletions with characteristic tradeoffs between NHEJ and Alt-EJ. (**A**–**D**) Deletion size profile at the AAVS1 locus relative to position of the DSB cut site. DNA-PK inhibitor (Nu7441, 1 μM) or CDK4/6 inhibitor (Palbociclib,1 μM) in (A) and (D). Isogenic WT and *LIG4*^{KO} and *POLQ*^{KO} cells created via CRISPR/Cas9 knockout in the HAP1 cell type background in (B) and (C). Single representative experiment shown (n = 3). (**E**, **F**) Deletion frequency by deletion length in isogenic HAP1 WT, LIG4^{KO} and POLQ^{KO} cells in E and in HEK293T cells with or without DNA-PK inhibition (Nu7441, 1 μM) in (F). Mean ± SEM in three experiments shown. (**G**) NHEJ repair events, defined as deletions 1–5 bp in size and normalized to the wild type condition in HAP1 and HEK293T cells. Mean ± SEM in 3–4 experiments shown. (**H**) Alt-EJ repair events, defined as deletions >5 bp and utilizing >2 bp of microhomology and normalized to the wild type condition. Mean ± SEM in 3–4 experiments shown. (**I**) Panel of eight cell lines and distribution of deletions by size. Asterisks signify t-tests as follows: * $P < 0.05$, ** $P < 0.01$, *** $P < 0.001$, **** $P < 0.0001$.

break based Rational InDel MetaAnalysis (RIMA) assay (17). *Polq*^{KO} in mouse embryonic stem cells also show only a partial reduction of deletions with >3 bp MH (30). Similarly, MH based deletions were only about 50% less frequent in *Polq*^{KO} cells compared to *POLQ* complemented cells in mouse embryonic fibroblasts (13). In this assay system, *POLQ*^{KO} clones in HAP1 and U2OS cells, also resulted in only a 50% decrease in the characteristic 12 bp Alt-EJ deletion (Figure 3F). Additional mechanisms, independent of Pol θ, may contribute to Alt-EJ. RAD52 is a known mediator of the Single Strand Annealing (SSA) pathway, which is mechanistically similar to Alt-EJ in using an annealed intermediate but uses larger homology stretches (>20 bp) compared to Alt-EJ (2–20 bp) leading to larger deletions (31). To determine possible alternative annealing mechanisms that facilitate Alt-EJ, we examined two *RAD52* knockout cell line pairs. We saw no reduction in Alt-EJ usage, as defined by the short-range 12 bp deletion, in two different *RAD52*^{KO} isogenic pairs in HAP1 and U2OS cells (Figure 3F). This result suggests RAD52 is likely not required for the smaller 12 bp deletion with 5 bp MH and is supported by a recently published report of differences in homology size usage between Pol θ mediated Alt-EJ and RAD52 mediated SSA (20).

SSTR requires resection and BRCA1 but is BRCA2 independent

To capture homologous recombination simultaneously with NHEJ and Alt-EJ, a 121 bp single strand oligonucleotide donor (ssODN) was used homologous to the breaksite containing 3 mutations in addition to the Cas9 directed at the

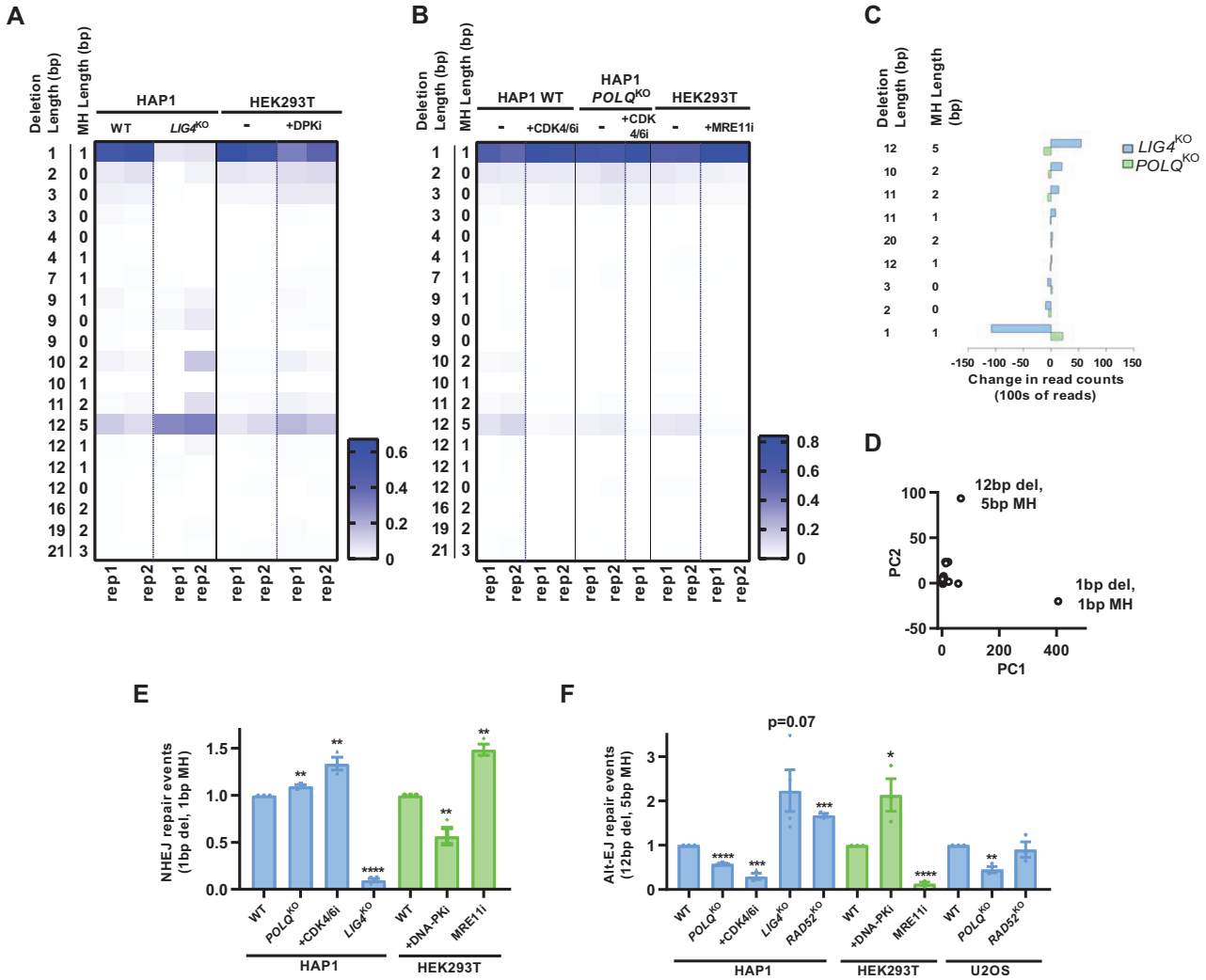

Figure 3. Single characteristic reads for each pathway represent most Alt-EJ and NHEJ-specific information. (**A**) Heat map of the most frequent 20 reads containing a deletion or insertion. In wild type cells, a 1 bp deletion is most common which is also heavily suppressed in a LIG4 knockout context or with pharmacologic inhibition of DNA-PK. A 12 bp deletion with 5 bp of surrounding microhomology is induced in these same contexts. (**B**) The 12 bp deletion with 5 bp of microhomology is dependent upon polymerase theta (*POLQ*) and cell cycle dependent (CDK4/6 inhibition) and relies on MRE11 implying a resection-mediated process. (**C**) Specific reads which depend upon LIG4 or POLQ. (**D**) Principal component analysis of reads most discriminating between NHEJ and Alt-EJ. (**E-F**) Quantification of the 1bp and 12 bp/5 bp MH read normalized to the WT condition. Mean ± SEM from 3–4 experiments shown. Asterisks signify *t*-tests as follows: * $P < 0.05$, ** $P < 0.01$, *** $P < 0.001$, **** $P < 0.0001$.

AAVS1 site. Two of these mutations were present at the PAM site to prevent Cas9 from cutting the donor template. ssODN integration was significantly decreased when cells were treated with an MRE11i or restricted in the G1 phase by CDK4/6 inhibition (Figure 4A). This supports that SSTR, the mechanism often used to describe CRISPR mediated edits using a ssODN, is dependent on MRE11 and is inhibited during the G1 phase of the cell cycle. Additionally, ssODN integration is likely BRCA1 dependent, as BRCA1-deficient HCC1937 cells were defective in the ssODN uptake, but upon complementation with BRCA1 we observed increased donor integration (Figure 4B).

Previous studies using I-SceI breaks have shown that single-strand templated repair (SSTR) is Rad51-independent in yeast (32). A recent publication also supports a Rad51-independent mechanism for SSTR after Cas9 breaks, and has found that SSTR is dependent on Rad52, Rad59, Srs2 and the Mre11-Rad50-Xrs2 (MRX) complex in yeast (33). Similarly, a CRISPR screen for SSTR suggests no involvement of RAD51 and BRCA2 in ssODN integration (34). Also, knockdown of BRCA1 or RAD51 in U2OS cells did not change levels of donor integration using ssODN (35). In corroboration with these published results, there were no changes in ssODN integration in DLD-1 *BRCA2*^{KO} cells compared to the isogenic DLD-1 WT control cells (Figure 4C). These results imply that SSTR used in Cas9 gene editing is independent of BRCA2 and could differ from traditional HR which requires BRCA2-assisted loading of RAD51 for successful repair. It follows that a double stranded donor would better represent and measure RAD51-mediated HR.

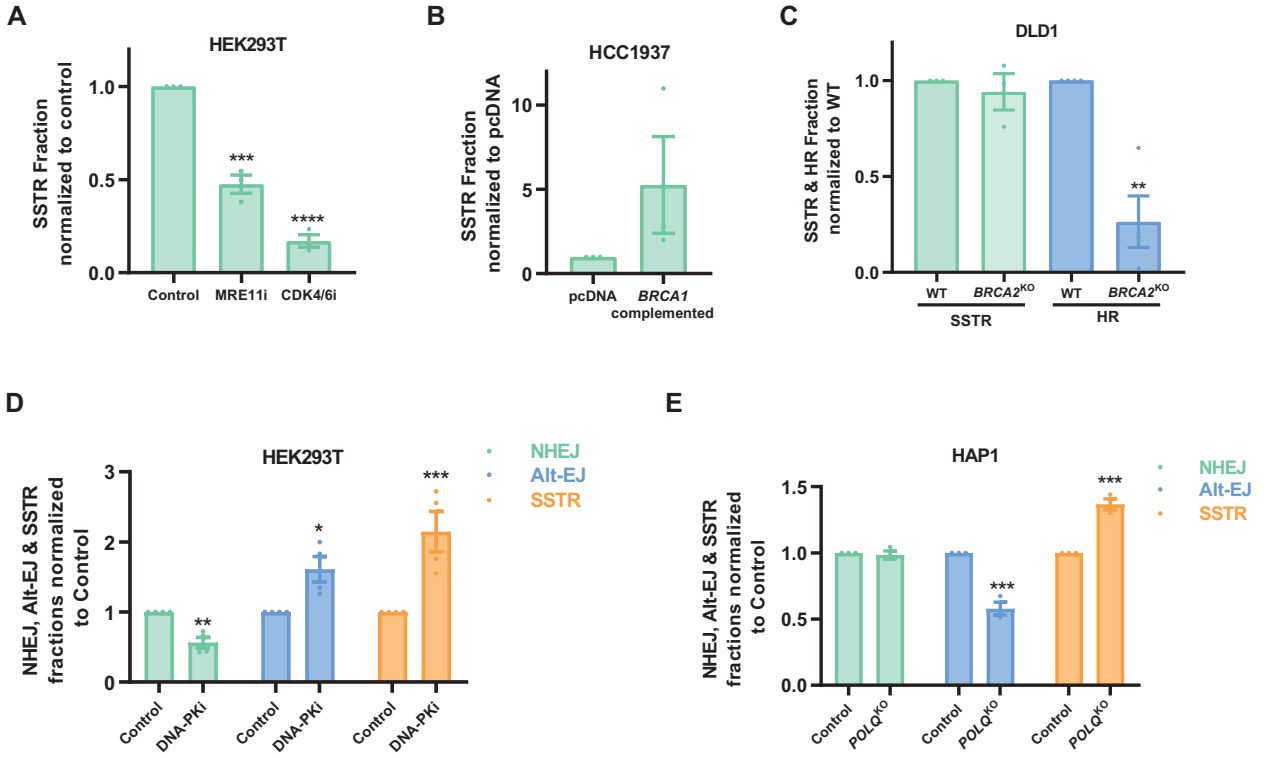

Figure 4. SSTR depends upon resection and BRCA1 but is BRCA2 independent. (**A**, **B**) SSTR (measured by three substitutions using a 121 bp single stranded donor) in HEK293T cells treated with 25 μM Mirin (MRE11i) and Palbociclib (CDK4/6i) and in isogenic pairs of HCC1937 BRCA1 deficient (pcDNA3.1) and BRCA1 complemented HCC1937 (BRCA1 complemented). (**C**) SSTR & HR (measured by three substitutions using the pUC57 plasmid containing a double stranded 121 bp sequence) in DLD1 WT and DLD1 BRCA2KO cells. (**D**, **E**) NHEJ, Alt-EJ and SSTR measured simultaneously in HEK293T cells treated with 1 μM NU7441 (DNA-PKi) and in isogenic HAP1 WT and HAP1 POLQKO cells. Mean ± SEM from 3–4 experiments shown. Asterisks signify *t*-tests as follows: * $P < 0.05$, ** $P < 0.01$, *** $P < 0.001$, **** $P < 0.0001$.

To verify if a dsDonor will be more representative of BRCA2 mediated conventional HR, we tested donor integration of a plasmid-based donor containing the same 121 bp sequence as the ssODN in the DLD-1 isogenic pairs. As expected, we observed that DSTR (Double strand templated repair) was dependent on BRCA2 for donor integration, supporting the notion that a double stranded donor is more representative of conventional HR (Figure 4C). The efficiency of HR in this system could likely be increased by lengthening the homology arms in the double stranded donor templates, as observed by other groups (36,37).

When we treated HEK293T cells with a DNA-PK inhibitor, we observed a significant enhancement in ssODN integration (SSTR) (Figure 4D). We also saw a concomitant increase in Alt-EJ, when NHEJ was inhibited by the DNA-PK inhibitor (Figure 4D). Similarly, with the inhibition of Alt-EJ in *POLQ*^{KO} cells, there was a significant increase in ssODN integration; however, NHEJ remained mostly unchanged suggesting that breaks which can't be repaired by Alt-EJ are preferably channeled into resection-mediated SSTR/HR pathways (Figure 4E).

Simplifying measurement of NHEJ, Alt-EJ, and HR reads using droplet digital PCR (ddPCR)

As shown in Figures 3 and 4, NHEJ, Alt-EJ and HR outputs can be measured using the frequency of their single characteristic reads of 1 bp deletion, 12 bp deletion with 5 bp MH and 3 bp mutations respectively. To simplify the measurement of these pathways we converted it to a direct droplet digital PCR application, wherein we designed unique probes to capture each characteristic read (Figure 5A & Methods section). The advantages of ddPCR over traditional PCRs is that it allows for absolute quantification of a particular read, without the need for internal standards. The droplet digital format separates genomic DNA into thousands of individual PCR reactions. The enzyme BamHI was used to specifically cut the genomic DNA into the region targeted for amplification for the ddPCR reaction. A Reference (REF) probe within the PCR amplified region, but away from the break site helps in quantifying the actual number of droplets containing our region of interest. The primers and probes were validated using ssDNA, which contained deletions for each probe and data was normalized to the mutant reads found by calculating the drop-off of the WT probe and presence of the Ref probe in the droplets.

We tested the use of these primers and probes with various pathway controls. With the Alt-EJ ddPCR signal, we found a similar decrease of signal in *POLQ*^{KO} clones as seen by the NGS technology (Figure 5B and C). Similarly, the HR/SSTR probe was able to capture the increase in reads observed after BRCA1 complementation in HCC1937 cells (Figure 5D and E). The NHEJ probe represented the loss of the signal after *LIG4*^{KO} in HAP1 cells (Figure 5F and G).

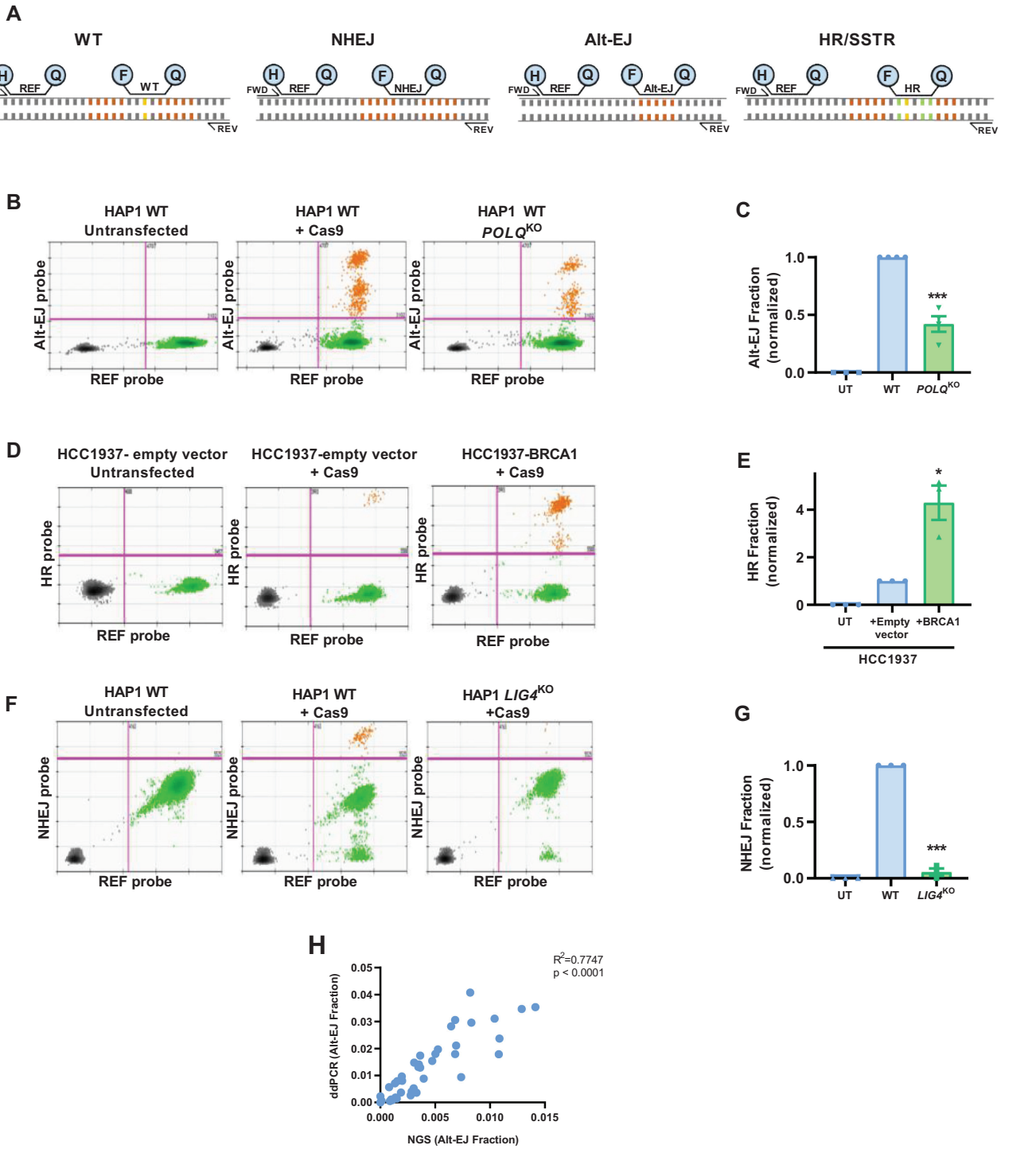

Figure 5. Measurement of specific NHEJ, Alt-EJ, and HR reads by ddPCR. (**A**) Schematic of primer/probe sets matching each specific read. H stands for the HEX probe, F for the FAM probe, Q for the quencher, and REF is the reference probe. The orange bases represent the 5 bp MH which is deleted in the Alt-EJ read and the yellow base represents the 1 bp deleted in the NHEJ read and the green bases are the substitutions introduced in the HR read. (**B**, **D**, **F**) Examples of 2D plots of droplet fluorescence. X axis represents the reference probe intensity. Y axis represents the Alt-EJ (B), HR (D) and NHEJ (F) fluorescent probe intensity. (**C**, **E**, **G**) Quantification of pathway shifts with ddPCR. Data normalized to the WT condition. Mean ± SEM of 3–4 experiments shown. (**H**) Correlation between Alt-EJ fraction from multiple samples obtained using ddPCR and NGS. Asterisks signify *t*-tests as follows: * $P < 0.05$, ** $P < 0.01$, *** $P < 0.001$, **** $P < 0.0001$.

When we compared the Alt-EJ signal obtained from NGS and ddPCR across multiple samples and cell lines, we found a significant correlation (Figure 5H). Thus, we were able to measure each pathway individually using a ddPCR platform, increasing the availability of the assays to laboratories that do not have access to NGS technology.

BRCA1 has a participatory role in Alt-EJ

The role of BRCA1 in Alt-EJ has been previously investigated with varying conclusions. BRCA1 forms a complex with resection factors such as CTIP/MRN and increases resection speed (38). In chicken DT40 cells, BRCA1 knockout and a CTIP S327A mutant deficient in complex formation with BRCA1 do not show a major effect on Alt-EJ using a linearized plasmid rejoining assay (39). Separately, the CTIP S326A had no effect on HR or Alt-EJ (40). BRCA1 and CTIP are required for alternative end-joining at uncapped telomeres and also for repair of Top2A-conjugated breaks created by etoposide (41,42). However, by the EJ2-GFP system, knockdown of BRCA1 by siRNA has been shown to both increase or decrease Alt-EJ (43,44). Interestingly, BRCA1 mediated a 4 bp MH Alt-EJ deletion in the EJ7 system only when the MH was embedded and needed 8 bp resection to be exposed, suggesting that BRCA1 could help mediate short range resection used for Alt-EJ (43).

To clarify these observations, we evaluated the role of BRCA1 in Alt-EJ by performing BRCA1 knockdown in U2OS cells using si-RNA. On performing the assay using si-BRCA1, we observed about ∼50% decrease in the Alt-EJ read-out (12 bp deletion with 5 bp MH) and a slight increase in the NHEJ readout (1bp deletion) (Figure 6A-C). Similarly, there was a 50% decrease in the Alt-EJ signal on BRCA1 knockdown using the EJ-2 system (Figure 6D). This is supported by a recent publication which also shows a 50% decrease in Alt-EJ using the EJ-2 system and further shows BRCA1 to have an important role in short range resection (43). Also, BRCA1-complemented HCC1937 cells had a significant increase in Alt-EJ compared to their BRCA1-deficient counterpart (Figure 6C). Conversely, BRCA2 knockout in DLD-1 cells led to an expected increase in the Alt-EJ read-out (Figure 6E and F) as expected (3,44–47). As BRCA1 seems to be important in mediating a 12 bp deletion in our assay system, we suggest that BRCA1 plays a participatory role in Alt-EJ unlike BRCA2 loss which upregulates Alt-EJ at two-ended DSBs.

Since other data, sometimes conflicting, suggests a suppressive role of BRCA1 on Alt-EJ, we sought to test our conclusion by interrogating cancer genomes to quantify Alt-EJ like genomic scars in cancer genomes with biallelic *BRCA1* and *BRCA2* mutations. The data available on 2780 whole genomes in the Pan-Cancer Analysis of Whole Genomes (PCAWG) project allowed us to empirically identify various mutational signatures to be significantly associated with *BRCA1/2* tumors. We looked for five different signatures covering signatures broadly associated with HR deficiency (HRD) as well as signatures which can be ascribed to Alt-EJ and NHEJ based on the length of deletions and MH usage. Large-scale state transitions (LST), chromosomal breaks leading to copy number alterations, and single base substitution pattern 3 (SBS3), signature identified by a flat distribution of base substitutions, are both signatures indicative of HRD and were not significantly different between *mBRCA1* and *mBRCA2* groups (Figure 6H and I).

If BRCA1 loss suppresses Alt-EJ in contrast to BRCA2 loss, we would expect a differential proportion of MH-containing, Alt-EJ-like deletions. The ID6 signature represents frequent deletions > 5 bp with MH mostly of 2 or more base pairs and thus is similar to an Alt-EJ scar seen *in vitro*. The ID8 signature contains frequent deletions > 5 bp in size, but with 0–1 bp of MH, which is similar to NHEJ events in MH size requirements but differs in the length of deletion. As expected, m*BRCA1* tumors show increased deletions with <2 bp MH and significantly decreased deletions with >2 bp MH compared to m*BRCA2* tumors (Figure 6G). Supporting this differential length of MH usage, there is a higher proportion of ID8 events and lower proportion of ID6 events (Alt-EJ-like) in biallelic mutant *BRCA1* tumors compared to biallelic mutant *BRCA2* tumors (Figure 6J and K). Only *mBRCA1*, not *mBRCA2*, tumors exhibit increased ID8 events which is in accordance with increased 1 bp deletion after BRCA1 knockdown in U2OS cells (Figure 6K and B). Various groups have identified templated insertions (TINS), a combination of direct repeat and snapback insertions, as a highly specific mutational signature associated with Pol θ activity (13,48–50). We observe a slight but significantly increased TINS signature in *mBRCA2* compared to *mBRCA1* tumors, suggesting mBRCA2 tumors might have a greater reliance on Pol θ mediated Alt-EJ pathway compared to *mBRCA1* tumors. On studying reversion mutations in *BRCA* mutant tumors resistant to PARP inhibitors, two groups have independently shown *BRCA2* mutant tumors to have increased Alt-EJ based reversion deletions compared to *BRCA1* mutant tumors (51,52). These genomic scar observations support a model in which BRCA2 and BRCA1 have differing influences on Alt-EJ in the context of two-ended DSBs.

However, of note, m*BRCA1* tumors exhibit increased ID6 events relative to *BRCA1/2* wild-type tumors and had increased deletions with greater than 2 bp MH compared to the WT group (Figure 6D, E & Supplementary Figure S2C), suggesting there is additional complexity with deletion events arising through carcinogenesis compared to two-ended Cas9-generated breaks. BRCA1's influence on Alt-EJ usage in replication-associated DSBs may differ from the two-ended DSBs created through Cas9 or I-SceI.

DISCUSSION

Cas9-induced breaks have become a frequently used tool to study DNA double strand break repair. Blunt ends are more commonly created than staggered breaks with endogenous insults such as radiation from x-rays or gamma rays (53). Previous work with the I-SceI endonuclease and cassette reporters has indicated that even a slightly staggered end obviates the need for the Ku heterodimer in end-joining (8). Thus, when studying canonical NHEJ in reporter assays, a Trex2-I-Sce1 endonuclease combination is employed to create a purely blunt end (54). In this way, the mostly blunt-ended Cas9 cuts are advantageous in modeling pathway tradeoffs reflective of endogenous blunt ended breaks. At some Cas9 loci, staggered DNA breaks are created at the

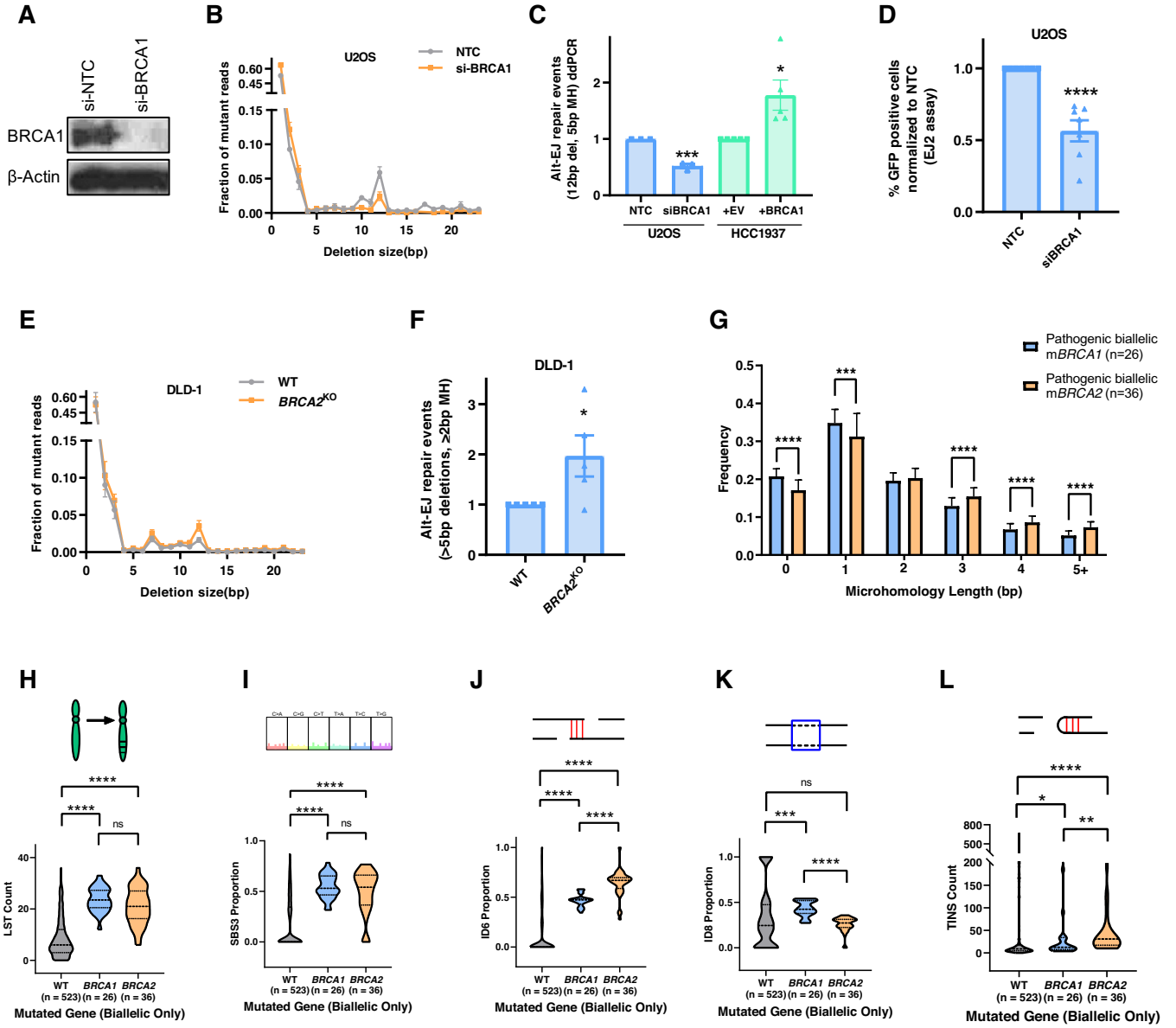

Figure 6. BRCA1 loss suppresses Alt-EJ. (**A**) Confirmation of BRCA1 knockdown in U2OS cells using si-BRCA1. Beta-actin is used as a loading control. (**B**) Deletion frequency by deletion length in U2OS cells treated with NTC and si-BRCA1 after Cas9 breaks at the AAVS1 locus. (**C**) Alt-EJ repair events in U2OS cells after BRCA1 knockdown as measured using the Alt-EJ ddPCR readout (blue). Alt-EJ by ddPCR in BRCA1-deficient HCC1937 cells complemented with either BRCA1 or empty vector (green). (**D**) Alt-EJ repair in U2OS cells after BRCA1 knockdown measured using the EJ-2 system. (**E**, **F**) Deletion frequency by deletion length and Alt-EJ repair events in isogenic DLD-1 WT and *BRCA2*^{KO} cell lines using NGS. (**G**) Frequency of deletions with varying microhomology lengths identified by the Pan-Cancer Analysis of Whole-Genomes (PCAWG) consortium in *BRCA1* and *BRCA2* biallelic mutated prostate, pancreatic, breast, and ovarian cancer patients. (**H–L**) Large-scale state transitions (LST) [H], single base substitution pattern 3 (SBS3) [I], ID6 [J], ID8 [K] and templated insertions (TINS) [L] signatures in WT, *BRCA1* biallelic mutated, and *BRCA2* biallelic mutated prostate, pancreatic, breast, and ovarian cancer patients. All *P*-values obtained through unpaired, two-tailed Mann–Whitney tests in GraphPad. Asterisks signify *t*-tests as follows: * $P < 0.05$, ** $P < 0.01$, *** $P < 0.001$, **** $P < 0.0001$.

–4 or –5 positions relative to the PAM site, which is manifested in NGS reads by 1 and 2 bp insertions generated by fill-in synthesis of the staggered end (55). The frequency of staggered end generation is heavily influenced by the –4 position nucleotide. In the locus presented here, the –4 position is occupied by a guanine, the least favorable nucleotide for staggered end generation (56–59) and thus we observe a very low frequency of 1 and 2 bp insertions.

In summary, using various pathway controls and by applying principal component analysis, we identified specific reads to differentiate Alt-EJ (12 bp with 5 bp MH) from NHEJ (1 bp). The Alt-EJ read fits with the recent publications describing Pol θ mediated end joining to require at least 4 bp MH and deletions to be within 15 bp on both sides of the break (9,13,60). Because both NHEJ and Alt-EJ can utilize short stretches of microhomology, we have utilized

a range of control experiments to empirically differentiate these pathways at an endogenous locus. The 1 bp, 1 bp MH read is over 90% reduced in a LIG4 knockout context and the 12 bp, 5 bp MH read is highly increased by LIG4 knockout and DNA-PK inhibition, supporting an Alt-EJ read. We do not rule out that there may be additional pathways and/or slight overlap between pathways in their repair end-products.

This assay provides a robust way of measuring Alt-EJ and gives the ability to capture multiple DSB repair pathways simultaneously. Importantly, the reads are converted to a ddPCR readout, which makes the assay more accessible without the need for sequencing and bioinformatic analysis. The assay can be used to quickly test DSB repair-related variables in isogenic cell line pairs, such as gene knockouts, mutations, and other cancer-specific alterations or test pathway choice effects of pharmacological agents. The advent of genome editing has increased the availability of these isogenic cell line pairs in mammalian cell line backgrounds, in some cases obviating the need to make gene knockout mice to generate murine embryonic fibroblasts.

Using this approach, the results presented here provide additional information to help clarify the role of BRCA1 in alternative end-joining. BRCA1 is understood to involve a pro-resection role, through cooperation with the MRN complex and CTIP (38) and/or chromatin remodeling and displacement of resection-inhibiting 53BP1 (61–63). Alt-EJ requires end-resection and it follows plausibly that BRCA1 does have a positive role in Alt-EJ, however there is conflicting data using cassette reporters (39,44) and BRCA1 as well as BRCA2 loss is synthetically lethal with Pol θ (2). Using two methods, the EJ2-GFP cassette reporter with an I-SceI induced break and the amplicon sequencing after a Cas9 break, we find that BRCA1 promotes Alt-EJ, even for very short range deletions such as this 12 bp microhomology-mediated endjoining event. The Alt-EJ misrepair event is likewise inhibited by Mre11 inhibition and G1 arrest, supporting the requirement of short-range resection. Thus, it is concluded that at least for two ended breaks created by endonucleases, BRCA1 promotes Alt-EJ.

One limitation of the technique is that it is unable to capture NHEJ repair reads which are repaired back to the WT sequence. Another drawback is that while a donor is introduced to quantify HR, we are unable to measure HR repair events formed by repair by the sister chromatid template. Moreover, the introduction of a donor sequence, in some cases, can affect the NHEJ:Alt-EJ ratio. Based on this observation, we recommend that NHEJ and Alt-EJ are reported without the introduction of the donor. Also, like other DSB repair assays, cell cycle differences can affect HR and Alt-EJ usage in this system. Factors that suppress cell growth also indirectly suppress the S/G2 dependent pathways (HR/Alt-EJ). However, a *POLQ* knockout in this assay suppresses Alt-EJ and increases HR (Figure 4E) – two readouts that give confidence that the *POLQ* observation is not confounded by suppression of cell growth and reduced S/G2 fractions. Importantly, the assay is useful in monitoring shift patterns in all 3 pathways consecutively as can be seen in the various examples demonstrated in this paper (Figure 4D and E).

DATA AVAILABILITY

Code used to process the FASTQ files obtained after NGS can be obtained at GitHub (https://github.com/cjsifuen/delmh).

SUPPLEMENTARY DATA

Supplementary Data are available at NAR Online.

ACKNOWLEDGEMENTS

We acknowledge the use of the Integrated Genomics Operation Core, funded by the National Cancer Institute's Cancer Center Support Grant [CCSG, P30 CA08748], Cycle for Survival, and the Marie-Josée and Henry R. Kravis Center for Molecular Oncology. We acknowledge Christopher Thompson for his assistance with figure design and other members of the Powell laboratory for their collaboration.

FUNDING

National Cancer Institute [R33 CA236670-01A1]; Emerson Collective Cancer Research Fund; American Association for Cancer Research AstraZeneca START fellowship [19-40-12-HUSS]; Cancer Center Support Grant of the National Institutes of Health/National Cancer Institute [P30CA008748, in part]; the content is solely the responsibility of the authors and does not necessarily represent the official views of the National Institutes of Health. Funding for open access charge: National Cancer Institute [R33 CA236670-01A1]; Emerson Collective Cancer Research Fund; American Association for Cancer Research AstraZeneca START fellowship [19-40-12-HUSS]; Cancer Center Support Grant of the National Institutes of Health/National Cancer Institute [P30CA008748, in part].
Conflict of interest statement. D.S.H. and S.S.H. are listed as inventors on a provisional patent filed by their institution related to the method used. There are no licenses or royalties.

REFERENCES

1. Delaney,G., Jacob,S., Featherstone,C. and Barton,M. (2005) The role of radiotherapy in cancer treatment: estimating optimal utilization from a review of evidence-based clinical guidelines. *Cancer*, **104**, 1129–1137.
2. Mateos-Gomez,P.A., Gong,F., Nair,N., Miller,K.M., Lazzerini-Denchi,E. and Sfeir,A. (2015) Mammalian polymerase θ promotes alternative NHEJ and suppresses recombination. *Nature*, **518**, 254–257.
3. Ceccaldi,R., Liu,J.C., Amunugama,R., Hajdu,I., Primack,B., Petalcorin,M.I., O'Connor,K.W., Konstantinopoulos,P.A., Elledge,S.J., Boulton,S.J. *et al.* (2015) Homologous-recombination-deficient tumours are dependent on Polθ-mediated repair. *Nature*, **518**, 258–262.
4. Leeman,J.E., Li,Y., Bell,A., Hussain,S.S., Majumdar,R., Rong-Mullins,X., Blecua,P., Damerla,R., Narang,H., Ravindran,P.T. *et al.* (2019) Human papillomavirus 16 promotes microhomology-mediated end-joining. *Proc. Natl. Acad. Sci. U.S.A.*, **116**, 21573–21579.
5. Liu,Q., Ma,L., Jones,T., Palomero,L., Pujana,M.A., Martinez-Ruiz,H., Ha,P.K., Murnane,J., Cuartas,I., Seoane,J. *et al.* (2018) Subjugation of TGFbeta signaling by human papilloma virus in head and neck squamous cell carcinoma shifts DNA repair from

homologous recombination to alternative end joining. *Clin. Cancer Res.*, **24**, 6001–6014.
6. Liu,Q., Palomero,L., Moore,J., Guix,I., Espin,R., Aytes,A., Mao,J.H., Paulovich,A.G., Whiteaker,J.R., Ivey,R.G. *et al.* (2021) Loss of TGFbeta signaling increases alternative end-joining DNA repair that sensitizes to genotoxic therapies across cancer types. *Sci. Transl. Med.*, **13**, eabc4465.
7. Pierce,A.J., Johnson,R.D., Thompson,L.H. and Jasin,M. (1999) XRCC3 promotes homology-directed repair of DNA damage in mammalian cells. *Genes Dev.*, **13**, 2633–2638.
8. Bennardo,N., Cheng,A., Huang,N. and Stark,J.M. (2008) Alternative-NHEJ is a mechanistically distinct pathway of mammalian chromosome break repair. *PLoS Genet.*, **4**, e1000110.
9. Bhargava,R., Sandhu,M., Muk,S., Lee,G., Vaidehi,N. and Stark,J.M. (2018) C-NHEJ without indels is robust and requires synergistic function of distinct XLF domains. *Nat. Commun.*, **9**, 2484.
10. Soong,C.-P., Breuer,G.A., Hannon,R.A., Kim,S.D., Salem,A.F., Wang,G., Yu,R., Carriero,N.J., Bjornson,R., Sundaram,R.K. *et al.* (2015) Development of a novel method to create double-strand break repair fingerprints using next-generation sequencing. *DNA Repair (Amst.)*, **26**, 44–53.
11. Bindra,R.S., Goglia,A.G., Jasin,M. and Powell,S.N. (2013) Development of an assay to measure mutagenic non-homologous end-joining repair activity in mammalian cells. *Nucleic Acids Res.*, **41**, e115.
12. Wyatt,D.W., Feng,W., Conlin,M.P., Yousefzadeh,M.J., Roberts,S.A., Mieczkowski,P., Wood,R.D., Gupta,G.P. and Ramsden,D.A. (2016) Essential roles for Polymerase θ-Mediated end joining in the repair of chromosome breaks. *Mol. Cell*, **63**, 662–673.
13. Carvajal-Garcia,J., Cho,J.-E., Carvajal-Garcia,P., Feng,W., Wood,R.D., Sekelsky,J., Gupta,G.P., Roberts,S.A. and Ramsden,D.A. (2020) Mechanistic basis for microhomology identification and genome scarring by polymerase theta. *Proc. Natl. Acad. Sci. U.S.A.*, **117**, 8476–8485.
14. van Overbeek,M., Capurso,D., Carter,M.M., Thompson,M.S., Frias,E., Russ,C., Reece-Hoyes,J.S., Nye,C., Gradia,S., Vidal,B. *et al.* (2016) DNA repair profiling reveals nonrandom outcomes at Cas9-mediated breaks. *Mol. Cell*, **63**, 633–646.
15. Chen,W., McKenna,A., Schreiber,J., Haeussler,M., Yin,Y., Agarwal,V., Noble,W.S. and Shendure,J. (2019) Massively parallel profiling and predictive modeling of the outcomes of CRISPR/Cas9-mediated double-strand break repair. *Nucleic Acids Res.*, **47**, 7989–8003.
16. Brinkman,E.K., Chen,T., de Haas,M., Holland,H.A., Akhtar,W. and van Steensel,B. (2018) Kinetics and fidelity of the repair of Cas9-induced double-strand DNA breaks. *Mol. Cell*, **70**, 801–813.
17. Taheri-Ghahfarokhi,A., Taylor,B.J.M., NitschLundin,R.,A., Cavallo,A.L., Madeyski-Bengtson,K., Karlsson,F., Clausen,M., Hicks,R., Mayr,L.M. *et al.* (2018) Decoding non-random mutational signatures at Cas9 targeted sites. *Nucleic Acids Res.*, **46**, 8417–8434.
18. Kent,T., Chandramouly,G., McDevitt,S.M., Ozdemir,A.Y. and Pomerantz,R.T. (2015) Mechanism of microhomology-mediated end-joining promoted by human DNA polymerase θ. *Nat. Struct. Mol. Biol.*, **22**, 230–237.
19. Ghezraoui,H., Piganeau,M., Renouf,B., Renaud,J.B., Sallmyr,A., Ruis,B., Oh,S., Tomkinson,A.E., Hendrickson,E.A., Giovannangeli,C. *et al.* (2014) Chromosomal translocations in human cells are generated by canonical nonhomologous end-joining. *Mol. Cell*, **55**, 829–842.
20. Kelso,A.A., Lopezcolorado,F.W., Bhargava,R. and Stark,J.M. (2019) Distinct roles of RAD52 and POLQ in chromosomal break repair and replication stress response. *PLos Genet.*, **15**, e1008319.
21. Treszezamsky,A.D., Kachnic,L.A., Feng,Z., Zhang,J., Tokadjian,C. and Powell,S.N. (2007) BRCA1- and BRCA2-deficient cells are sensitive to etoposide-induced DNA double-strand breaks via topoisomerase II. *Cancer Res.*, **67**, 7078–7081.
22. Natsume,T., Kiyomitsu,T., Saga,Y. and Kanemaki,M.T. (2016) Rapid protein depletion in human cells by auxin-inducible degron tagging with short homology donors. *Cell Rep.*, **15**, 210–218.
23. Alexandrov,L.B., Kim,J., Haradhvala,N.J., Huang,M.N., Tian Ng,A.W., Wu,Y., Boot,A., Covington,K.R., Gordenin,D.A., Bergstrom,E.N. *et al.* (2020) The repertoire of mutational signatures in human cancer. *Nature*, **578**, 94–101.
24. Campbell,P.J., Getz,G., Korbel,J.O., Stuart,J.M., Jennings,J.L., Stein,L.D., Perry,M.D., Nahal-Bose,H.K., Ouellette,B.F.F., Li,C.H. *et al.* (2020) Pan-cancer analysis of whole genomes. *Nature*, **578**, 82–93.
25. Popova,T., Manié,E., Rieunier,G., Caux-Moncoutier,V., Tirapo,C., Dubois,T., Delattre,O., Sigal-Zafrani,B., Bollet,M., Longy,M. *et al.* (2012) Ploidy and large-scale genomic instability consistently identify basal-like breast carcinomas with BRCA1/2 inactivation. *Cancer Res.*, **72**, 5454–5462.
26. Degasperi,A., Amarante,T.D., Czarnecki,J., Shooter,S., Zou,X., Glodzik,D., Morganella,S., Nanda,A.S., Badja,C., Koh,G. *et al.* (2020) A practical framework and online tool for mutational signature analyses show intertissue variation and driver dependencies. *Nat. Cancer*, **1**, 249–263.
27. Nik-Zainal,S., Davies,H., Staaf,J., Ramakrishna,M., Glodzik,D., Zou,X., Martincorena,I., Alexandrov,L.B., Martin,S., Wedge,D.C. *et al.* (2016) Landscape of somatic mutations in 560 breast cancer whole-genome sequences. *Nature*, **534**, 47–54.
28. Oksenych,V., Kumar,V., Liu,X., Guo,C., Schwer,B., Zha,S. and Alt,F.W. (2013) Functional redundancy between the XLF and DNA-PKcs DNA repair factors in V(D)J recombination and nonhomologous DNA end joining. *Proc. Natl. Acad. Sci. U.S.A.*, **110**, 2234–2239.
29. Huertas,P. and Jackson,S.P. (2009) Human CtIP mediates cell cycle control of DNA end resection and double strand break repair. *J. Biol. Chem.*, **284**, 9558–9565.
30. Schimmel,J., Kool,H., van Schendel,R. and Tijsterman,M. (2017) Mutational signatures of non-homologous and polymerase theta-mediated end-joining in embryonic stem cells. *EMBO J.*, **36**, 3634–3649.
31. Bhargava,R., Onyango,D.O. and Stark,J.M. (2016) Regulation of single-strand annealing and its role in genome maintenance. *Trends Genet.*, **32**, 566–575.
32. Storici,F., Snipe,J.R., Chan,G.K., Gordenin,D.A. and Resnick,M.A. (2006) Conservative repair of a chromosomal double-strand break by single-strand DNA through two steps of annealing. *Mol. Cell. Biol.*, **26**, 7645–7657.
33. Gallagher,D.N., Pham,N., Tsai,A.M., Janto,A.N., Choi,J., Ira,G. and Haber,J.E. (2020) A Rad51-independent pathway promotes single-strand template repair in gene editing. *PLoS Genet.*, **16**, e1008689.
34. Richardson,C.D., Kazane,K.R., Feng,S.J., Zelin,E., Bray,N.L., Schäfer,A.J., Floor,S.N. and Corn,J.E. (2018) CRISPR-Cas9 genome editing in human cells occurs via the Fanconi anemia pathway. *Nat. Genet.*, **50**, 1132–1139.
35. Bothmer,A., Phadke,T., Barrera,L.A., Margulies,C.M., Lee,C.S., Buquicchio,F., Moss,S., Abdulkerim,H.S., Selleck,W., Jayaram,H. *et al.* (2017) Characterization of the interplay between DNA repair and CRISPR/Cas9-induced DNA lesions at an endogenous locus. *Nat. Commun.*, **8**, 13905.
36. Zhang,J.P., Li,X.L., Li,G.H., Chen,W., Arakaki,C., Botimer,G.D., Baylink,D., Zhang,L., Wen,W., Fu,Y.W. *et al.* (2017) Efficient precise knockin with a double cut HDR donor after CRISPR/Cas9-mediated double-stranded DNA cleavage. *Genome Biol.*, **18**, 35.
37. Lin,S., Staahl,B.T., Alla,R.K. and Doudna,J.A. (2014) Enhanced homology-directed human genome engineering by controlled timing of CRISPR/Cas9 delivery. *Elife*, **3**, e04766.
38. Cruz-García,A., López-Saavedra,A. and Huertas,P. (2014) BRCA1 accelerates CtIP-mediated DNA-end resection. *Cell Rep.*, **9**, 451–459.
39. Yun,M.H. and Hiom,K. (2009) CtIP-BRCA1 modulates the choice of DNA double-strand-break repair pathway throughout the cell cycle. *Nature*, **459**, 460–463.
40. Reczek,C.R., Szabolcs,M., Stark,J.M., Ludwig,T. and Baer,R. (2013) The interaction between CtIP and BRCA1 is not essential for resection-mediated DNA repair or tumor suppression. *J. Cell Biol.*, **201**, 693–707.
41. Badie,S., Carlos,A.R., Folio,C., Okamoto,K., Bouwman,P., Jonkers,J. and Tarsounas,M. (2015) BRCA1 and CtIP promote alternative non-homologous end-joining at uncapped telomeres. *EMBO J.*, **34**, 410–424.
42. Aparicio,T., Baer,R., Gottesman,M. and Gautier,J. (2016) MRN, CtIP, and BRCA1 mediate repair of topoisomerase II-DNA adducts. *J. Cell Biol.*, **212**, 399–408.

43. Tsai,L.J., Lopezcolorado,F.W., Bhargava,R., Mendez-Dorantes,C., Jahanshir,E. and Stark,J.M. (2020) RNF8 has both KU-dependent and independent roles in chromosomal break repair. *Nucleic Acids Res.*, **48**, 6032–6052.
44. Ahrabi,S., Sarkar,S., Pfister,S.X., Pirovano,G., Higgins,G.S., Porter,A.C.G. and Humphrey,T.C. (2016) A role for human homologous recombination factors in suppressing microhomology-mediated end joining. *Nucleic Acids Res.*, **44**, 5743–5757.
45. Feng,W., Simpson,D.A., Carvajal-Garcia,J., Price,B.A., Kumar,R.J., Mose,L.E., Wood,R.D., Rashid,N., Purvis,J.E., Parker,J.S. *et al.* (2019) Genetic determinants of cellular addiction to DNA polymerase theta. *Nat. Commun.*, **10**, 4286.
46. Kais,Z., Rondinelli,B., Holmes,A., O'Leary,C., Kozono,D., D'Andrea,A.D. and Ceccaldi,R. (2016) FANCD2 maintains fork stability in BRCA1/2-deficient tumors and promotes alternative end-joining DNA repair. *Cell Rep.*, **15**, 2488–2499.
47. Eckelmann,B.J., Bacolla,A., Wang,H., Ye,Z., Guerrero,E.N., Jiang,W., El-Zein,R., Hegde,M.L., Tomkinson,A.E., Tainer,John A. *et al.* (2020) XRCC1 promotes replication restart, nascent fork degradation and mutagenic DNA repair in BRCA2-deficient cells. *NAR Cancer*, **2**, zcaa013.
48. van Schendel,R., van Heteren,J., Welten,R. and Tijsterman,M. (2016) Genomic scars generated by polymerase theta reveal the versatile mechanism of alternative end-joining. *PLos Genet.*, **12**, e1006368.
49. Schimmel,J., van Schendel,R., den Dunnen,J.T. and Tijsterman,M. (2019) Templated insertions: a smoking gun for polymerase theta-mediated end joining. *Trends Genet.*, **35**, 632–644.
50. Hwang,T., Reh,S., Dunbayev,Y., Zhong,Y., Takata,Y., Shen,J., McBride,K.M., Murnane,J.P., Bhak,J., Lee,S. *et al.* (2020) Defining the mutation signatures of DNA polymerase θ in cancer genomes. *NAR Cancer*, **2**, zcaa017.
51. Pettitt,S.J., Frankum,J.R., Punta,M., Lise,S., Alexander,J., Chen,Y., Yap,T.A., Haider,S., Tutt,A.N.J. and Lord,C.J. (2020) Clinical BRCA1/2 reversion analysis identifies hotspot mutations and predicted neoantigens associated with therapy resistance. *Cancer Discov*.
52. Tobalina,L., Armenia,J., Irving,E., O'Connor,M.J. and Forment,J.V. (2020) A meta-analysis of reversion mutations in BRCA genes identifies signatures of DNA end-joining repair mechanisms driving therapy resistance. *Ann. Oncol.*, **32**, 103–112.
53. Iliakis,G., Mladenov,E. and Mladenova,V. (2019) Necessities in the processing of DNA double strand breaks and their effects on genomic instability and cancer. *Cancers (Basel)*, **11**, 1671.
54. Bennardo,N., Gunn,A., Cheng,A., Hasty,P. and Stark,J.M. (2009) Limiting the persistence of a chromosome break diminishes its mutagenic potential. *PLoS Genet.*, **5**, e1000683.
55. Shou,J., Li,J., Liu,Y. and Wu,Q. (2018) Precise and predictable CRISPR chromosomal rearrangements reveal principles of Cas9-mediated nucleotide insertion. *Mol. Cell*, **71**, 498–509.
56. Leenay,R.T., Aghazadeh,A., Hiatt,J., Tse,D., Roth,T.L., Apathy,R., Shifrut,E., Hultquist,J.F., Krogan,N., Wu,Z. *et al.* (2019) Large dataset enables prediction of repair after CRISPR-Cas9 editing in primary T cells. *Nat. Biotechnol.*, **37**, 1034–1037.
57. Shen,M.W., Arbab,M., Hsu,J.Y., Worstell,D., Culbertson,S.J., Krabbe,O., Cassa,C.A., Liu,D.R., Gifford,D.K. and Sherwood,R.I. (2018) Predictable and precise template-free CRISPR editing of pathogenic variants. *Nature*, **563**, 646–651.
58. Allen,F., Crepaldi,L., Alsinet,C., Strong,A.J., Kleshchevnikov,V., De Angeli,P., Palenikova,P., Khodak,A., Kiselev,V., Kosicki,M. *et al.* (2018) Predicting the mutations generated by repair of Cas9-induced double-strand breaks. *Nat. Biotechnol.*, **37**, 64–72.
59. Chakrabarti,A.M., Henser-Brownhill,T., Monserrat,J., Poetsch,A.R., Luscombe,N.M. and Scaffidi,P. (2019) Target-specific precision of CRISPR-mediated genome editing. *Mol. Cell*, **73**, 699–713.
60. Yousefzadeh,M.J., Wyatt,D.W., Takata,K., Mu,Y., Hensley,S.C., Tomida,J., Bylund,G.O., Doublié,S., Johansson,E., Ramsden,D.A. *et al.* (2014) Mechanism of suppression of chromosomal instability by DNA polymerase POLQ. *PLos Genet.*, **10**, e1004654.
61. Densham,R.M., Garvin,A.J., Stone,H.R., Strachan,J., Baldock,R.A., Daza-Martin,M., Fletcher,A., Blair-Reid,S., Beesley,J., Johal,B. *et al.* (2016) Human BRCA1-BARD1 ubiquitin ligase activity counteracts chromatin barriers to DNA resection. *Nat. Struct. Mol. Biol.*, **23**, 647–655.
62. Chapman,J.R., Sossick,A.J., Boulton,S.J. and Jackson,S.P. (2012) BRCA1-associated exclusion of 53BP1 from DNA damage sites underlies temporal control of DNA repair. *J. Cell Sci.*, **125**, 3529–3534.
63. Kakarougkas,A., Ismail,A., Katsuki,Y., Freire,R., Shibata,A. and Jeggo,P.A. (2013) Co-operation of BRCA1 and POH1 relieves the barriers posed by 53BP1 and RAP80 to resection. *Nucleic Acids Res.*, **41**, 10298–10311.